FINAL REPORT (#DOE-ER46047-1)

PROJECT TITLE:

MEASUREMENTS AND COMPUTATIONS OF FUEL DROPLET TRANSPORT IN TURBULENT FLOWS.

DOE GRANT NO.: DE-FG02-03ER46047

PRINCIPAL INVESTIGATORS: JOSEPH KATZ AND OMAR KNIO

DEPARTMENT OF MECHANICAL ENGINEERING, THE JOHNS HOPKINS UNIVERSITY.

1. SUMMARY OF OBJECTIVES:

The objective of this project is to study the dynamics of fuel droplets in turbulent water flows. The results are essential for development of models capable of predicting the dispersion of slightly light/heavy droplets in isotropic turbulence. Since we presently do not have any experimental data on turbulent diffusion of droplets, existing mixing models have no physical foundations. Such fundamental knowledge is essential for understanding/modeling the environmental problems associated with water-fuel mixing, and/or industrial processes involving mixing of immiscible fluids.

The project has had experimental and numerical components:

1. The experimental part of the project has had two components. The first involves measurements of the lift and drag forces acting on a droplet being entrained by a vortex. The experiments and data analysis associated with this phase are still in progress, and the facility, constructed specifically for this project is described in Section 3. In the second and main part, measurements of fuel droplet dispersion rates have been performed in a special facility with controlled isotropic turbulence. As discussed in detail in Section 2, quantifying and modeling the of droplet dispersion rate requires measurements of their three dimensional trajectories in turbulent flows. To obtain the required data, we have introduced a new technique - high-speed, digital Holographic Particle Image Velocimetry (HPIV). The technique, experimental setup and results are presented in Section 2. Further information is available in Gopalan et al. (2005, 2006).

2. The objectives of the numerical part are: (1) to develop a computational code that combines DNS of isotropic turbulence with Lagrangian tracking of particles based on integration of a dynamical equation of motion that accounts for pressure, added mass, lift and drag forces, (2) to perform extensive computations of both buoyant (bubbles) and slightly buoyant (droplets) particles in turbulence conditions relevant to the experiments, and (3) to explore whether the corresponding predictions can explain the experimentally-observed behavior of the rise and dispersion of oil droplets in isotropic turbulence. A brief summary of results is presented in Section 4.

NOMENCLATURE

A_i	-	Acceleration of droplets in x, y or z direction
D_{ii}	-	Dispersion coefficient in x, y or z direction
D	-	Dispersion Tensor
G	-	Self part of intermediate scattering function
i	-	$\sqrt{-1}$
k	-	Wave number vector
L		Integral Time scale of turbulence
R_{ii}	-	Autocorrelation in x , y or z direction
Re_λ	-	Reynolds number based on Taylor scale
R_1	-	Droplet radii lies in bin 1 (0.15-0.3)mm
R_2	-	Droplet radii lies in bin 2 (0.3-0.45)mm
R_3	-	Droplet radii lies in bin 3 (0.45-0.6)mm
R_4	-	Droplet radii lies in bin 4 (0.6-0.75)mm
t		Time
T		Droplet diffusion time scale
t_k		Kolmogorov time scale $=(\nu/\varepsilon)^{0.5}$
U_i	-	Droplet or particle velocity fluctuation in x , y or z direction
u	-	Fluid velocity fluctuation (rms)
X	-	Particle trajectory
x, y ,z	-	Coordinate planes with y denoting depth
y	-	Distance (in dispersion tensor)
Y_i^2	-	Mean square displacement in x, y or z direction
ν		Kinematic viscosity of fluid
ε		Dissipation rate of turbulent flow
τ	-	Autocorrelation time

Subscripts

i	-	Component direction (x , y or z)

2. MEASUREMENTS OF FUEL DROPLET DISPERSION IN TURBULNT FLOWS

2.1 INTRODUCTION

Taylor's (1921) pioneering work on turbulent dispersion shows that diffusivity of a "fluid point" could be calculated from the Lagrangian autocorrelation function R_{ii},

$$R_{ii}(t) = \int u_i(t)u_i(t+\tau)dt \,/\, \int u_i^2(t)dt$$

where $u_i(t)$ is the velocity (see nomenclature for a complete list of variables). Droplets and particles do not follow the surrounding fluid so that their diffusion differs from that of the fluid points. Csanady (1963) surmises that the theory of Taylor remains valid for particles. Assuming a Fickian diffusion process, the dispersion coefficient may be estimated from

$$D_{ii}(\tau) = \overline{U_i^2}\int_0^{\tau} R_{ii}(t')dt'$$

and the mean square displacement or dispersion from

$$\overline{Y_i^2(\tau)} = 2\overline{U_i^2}\int_0^{\tau}\int_0^{t_1} R_{ii}(t')dt'\,dt_1$$

Snyder & Lumley's (1971) landmark experiments provide comprehensive direct measurements of the particle and fluid autocorrelation function, using hollow glass spheres for the fluid, and particles with different densities and diameters. They show that the magnitude of R_{ii} decreases and its decay rate increased with the particle density. They also show that prediction of diffusion by assuming that dispersion of particles in turbulent flows is proportional to the concentration gradient is fundamentally incorrect. Following the recent analysis of Moroni & Cushman (2001), dispersion may be represented in terms of a generalized, wave-vector and frequency dependent, dispersion tensor, $\mathbf{D}(\boldsymbol{y},\tau)$, where $\boldsymbol{y}$ is the distance, which enables the theory to accommodate various processes, including Fickian, convolution-Fickian, as well fractional-Fickian fluxes. As outlined by Moroni & Cushman (2001), the generalized dispersion tensor can be extracted by analyzing the evolution of the so-called self-part of the intermediate scattering function:

$$\hat{G}(\mathbf{k},\tau) = \left\langle e^{-i\mathbf{k}\cdot\mathbf{X}(0)} e^{i\mathbf{k}\cdot\mathbf{X}(\tau)} \right\rangle$$

where $\mathbf{k}$ is the wave number vector, $\mathbf{X}$ is the particle trajectory. If the Lagrangian trajectories were known over a suitable time interval, then the generalized dispersion tensor could be obtained by analyzing the evolution of $\overline{G}$. At large times, one would expect that the particle dispersion can be represented as a Fickian process, but in short times it may not. As both Taylor's (1921) and Cushman and Moroni (2001) work indicates, direct measurement of droplet dispersion requires data on the time history of the velocity along the 3-D trajectory of the droplets. To achieve this objective, we have introduced high-speed digital holography.

2.2 EXPERIMENTAL SETUP AND PROCEDURES

The facility shown in figure 1 generates nearly isotropic turbulence with weak mean flow by using four symmetrically located rotating grids. Each grid has a 40% blockage factor and they are attached to motors powered by variable frequency static inverters. The frequency of inverters can be adjusted to vary turbulence levels. Details of the facility are provided in Friedman and Katz (2002). The current experiments are performed at a mixer velocity of 225, 337 and 506 rpm and relevant parameters for this

speed are shown in table 1.0. The injected droplets are research grade diesel fuel that has a specific gravity of 0.85 and hence is slightly buoyant.

Table 1: Turbulence facility data

Mixer rpm	225	337.5	506.3
RMS Velocity (cm/s)	4.55 (4.04, 4.7, 4.91)*	6.6	9.4
Average Absolute Mean Velocity (cm/s)	0.65	1.5	2.0
Dissipation ε (m^2/s^3)	0.0017	0.0086	0.02
Taylor Microscale, λ (mm)	4.3	2.5	1.9
Kolmogorov Length Scale, η (mm)	0.156	0.088	0.065
Integral Length Scale, L (mm)	55	33	28
Taylor Scale Reynolds Number Re_λ	194	203	223

* Three components of RMS velocity fluctuations (u', v', w,) to demonstrate extent of anisotropy.

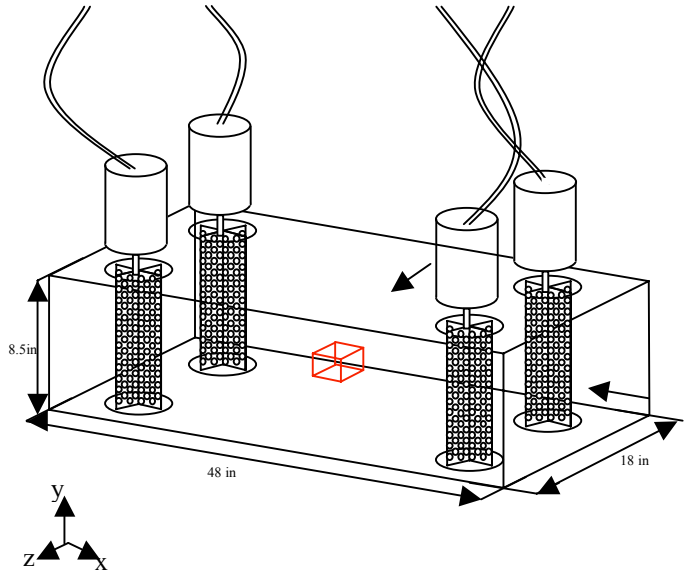

Figure 1: Isotropic Turbulence Generating Facility

Measurements of Mean Flow and Turbulence in the Facility: The mean flow in the x-y plane of the tank was measured using Particle Image Velocimetry (PIV). The optical setup is shown in the fig 2. The light source is a New Wave Research Nd-YAG laser and the pulse delay is 4 ms. For tracers we use 7-10 μm glass beads and the images were acquired using a Kodak ES4, 2k x 2k digital cameras with a 105mm lens. 1200 vector maps are added to obtain the mean flow and turbulence parameters. The mean flow is measured in steps of 2mm across the entire sample volume. The digital images are enhanced and velocity vector maps are determined using cross correlation analysis. Details of these procedures are available in Roth and Katz (2001). The uncertainty in instantaneous velocity is about 2%.

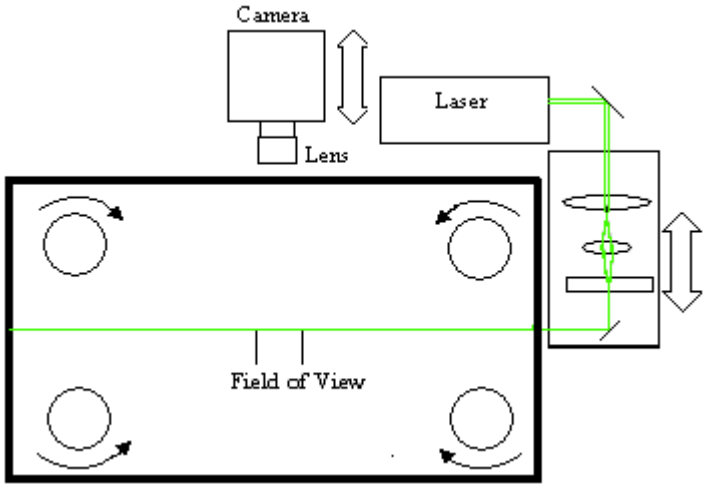

Fig. 2 Optical setup for the PIV measurements. The laser sheet is perpendicular to the page.

Droplets tracks measurement: Our objectives require measurements of the time history of the 3D trajectory. Holographic particle image velocimetry is the only technique to-date that can measure 3-D instantaneous velocity distribution over a sample volume with an extended depth (Barnhart et al. 1994, Malkiel et al. 2003, Zhang et al. 1997, Pu and Meng 2000, Tao et al. 2002, Sheng et al. 2003) The optical setup is shown in figure 3. We record two perpendicular holograms in order to maintain the same spatial resolution in all directions. The Light source is a Q switched Nd:Ylf diode pumped laser. The laser beam is passed through a spatial filter, a collimating lens and a beam splitter before illuminating the sample volume from two perpendicular directions. The lenses marked as L1 and L2 demagnify the beam by a 2.2:1 ratio. The images are acquired by two Photron 1k x 1k cameras with a pixel resolution of 17-μm at 250 frames/sec (maximum speed of 2000 frames/sec).

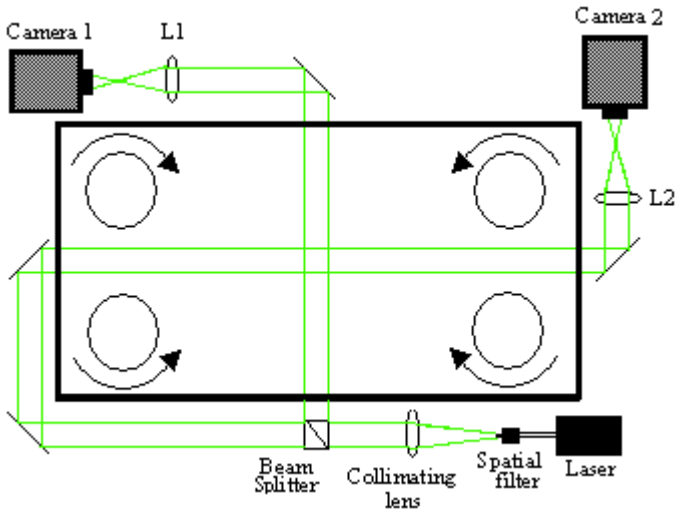

Figure 3: Optical setup for Digital Holographic PIV measurements.

The digital holograms are reconstructed numerically using the Fresnel approximation by convolving the intensity distribution with a source function. Details of the procedure are available in Malkiel et al (2003). To maintain a uniform background and to remove background effects we divide the image by the background image. We first track the 2-D projection of tracks separately and then match them to obtain 3-D coordinates of the droplets. Droplet spatial location is measured by

1) Multiple Thresholding
2) Using a circularity filter.

The depth location is acquired (within 5-6 mm) using maximum edge intensity.
Criteria for identifying the 2-D droplet tracks are:

1) Closest point in the next time step
2) Radius within a certain tolerance range
3) Depth within a certain tolerance range
4) Maximum acceleration
5) Avoiding very sharp unnatural jitter
6) Linear regression for the crossing of tracks

An automated code has been developed to track the droplets based on these criteria. The 2-D tracks are matched by finding the one with the least square difference between the common axes (vertical). Cross correlation analysis is then used for determining the velocity in order to get sub pixel accuracy. The velocity time series is low pass filtered to remove high frequency jitter. The mean velocity in the volume calculated using PIV is subtracted from each instantaneous velocity to obtain time history of droplet velocity fluctuations.

Fig 4 shows sample sections of the reconstructed image with the two orthogonal views next to each other, indicating the matched droplets. We can also see some seed particles in the background. Fig 5 shows the orthogonal 2-D tracks. An example of the 3-D tracks is shown in fig 6, and the velocities are displayed using color-coding.

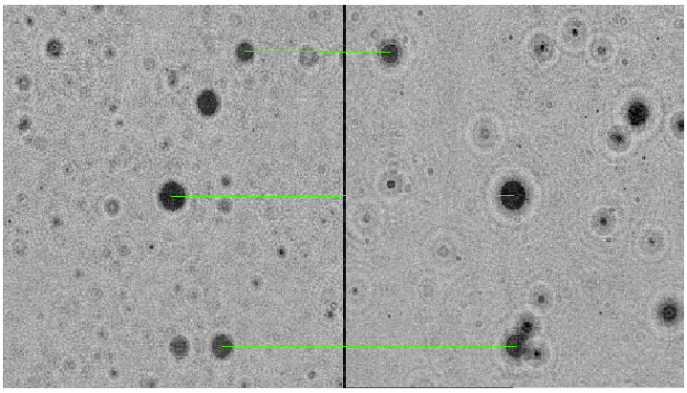

Fig. 4 Orthogonal reconstructed view of the droplets in isotropic turbulence with arrows showing particles

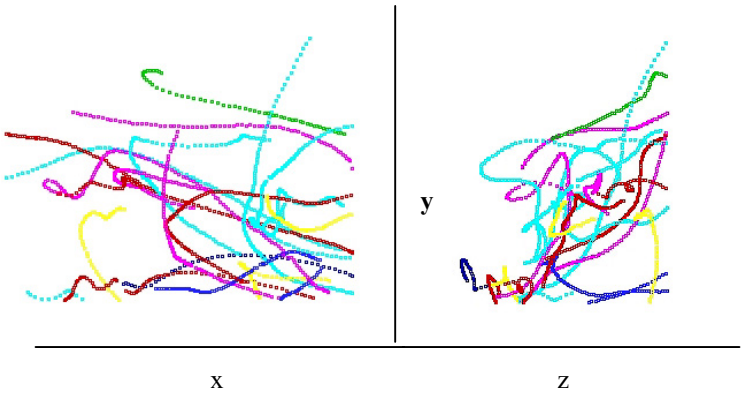

Figure 5: Sample droplet tracks in the two orthogonal views showing the matched portions color-coded.

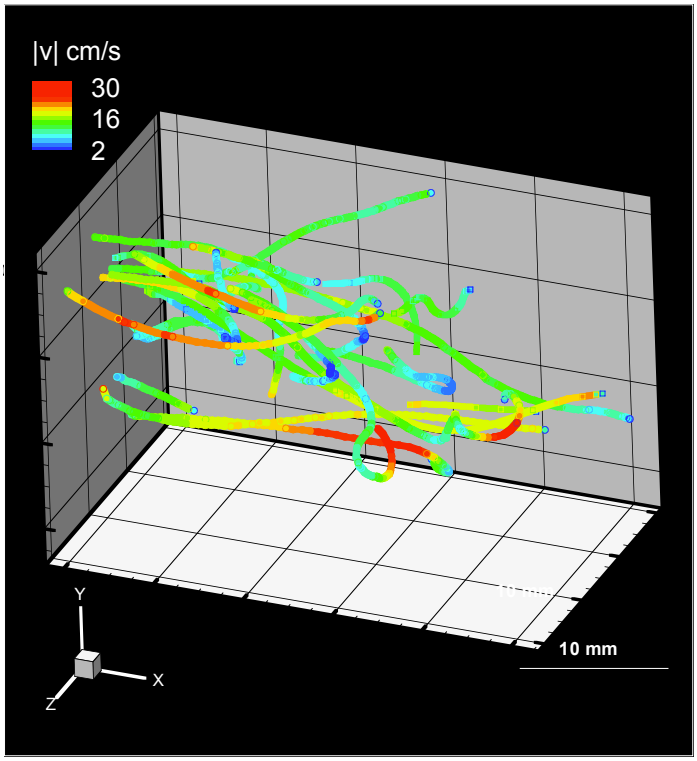

Fig. 6 3-D Sample 3D diesel droplet tracks with the velocity color coded.

Figure 7 shows the velocity time series for one of the droplets as raw data, i.e. before any low-pass filter is applied . This indicates the accuracy of the measurements

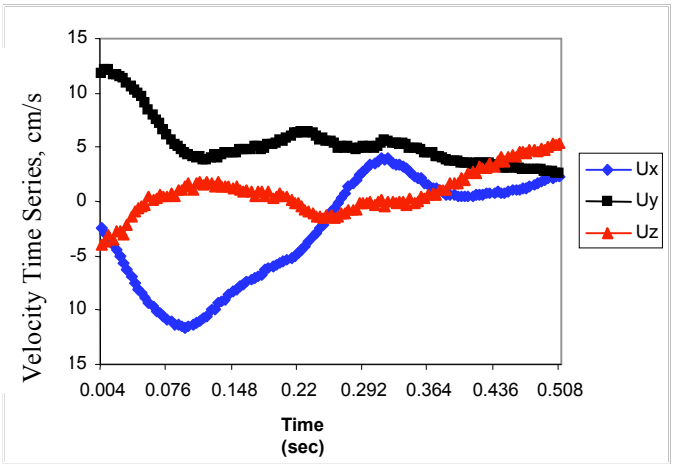

Figure 7: Sample three components of velocity time series of a droplet.

2.3 RESULTS AND DISCUSSION

Droplet statistics are grouped into four bins based on their radii. The bin R_1 contains 0.15-0.3mm radius droplets, bin R_2 contains 0.3-0.45mm droplets, bin R_3 contains 0.45-0.6mm droplets and bin R_4 contains 0.6-0.75mm droplets. Figure 8 shows the number of measured tracks for each of the four radii bin considered as a function of time that the track remains with the field of view. The droplet size varies from twice to a maximum of ten times the Kolmogorov scale. It is evident that tracking it for a period exceeding 0.3 sec increases for larger droplets. The reason is associated with the tracking algorithm and the location of the injector. As the droplet size increases it is easier to track it even when trajectories cross each other. We are going to modify our automated tracking program to track small size droplets more efficiently. Also due to the position of the injection needle (one cm below field of view) a lot of small droplets enter the viewing region near the edge and hence could be tracked only for a smaller time.

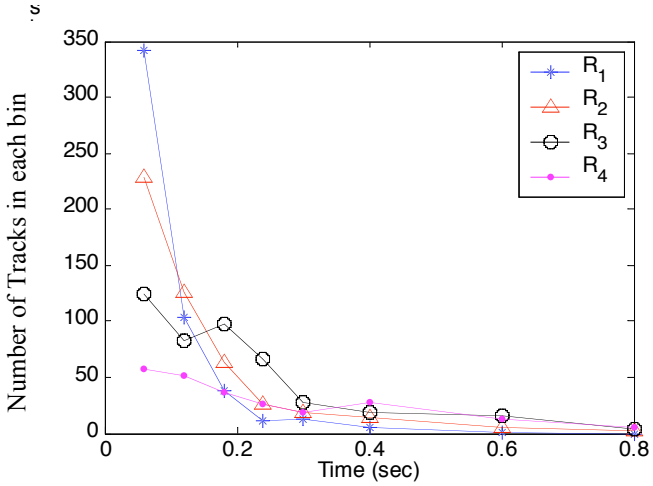

Figure 8: Histograms of track length for different bins of radii (225 rpm).

The PDF of the velocity and acceleration for the entire dataset are shown in figure 9 and 10. The velocity PDF closely resembles the Gaussian distribution although the mode does not exactly correspond with the mean. This might be due to the limited dataset not being converged. The acceleration PDF clearly

deviates from the Gaussian distribution. The wide tail tells us that the droplets acceleration experiences more intermittent fluctuations than velocities, as is generally observed for fluid flow data.

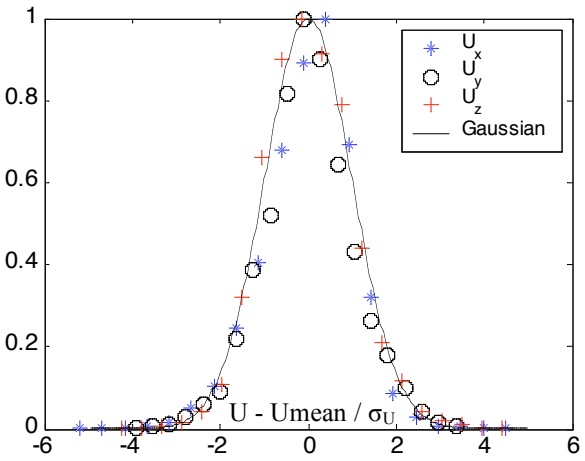

Figure 9: PDF of combined velocity data.

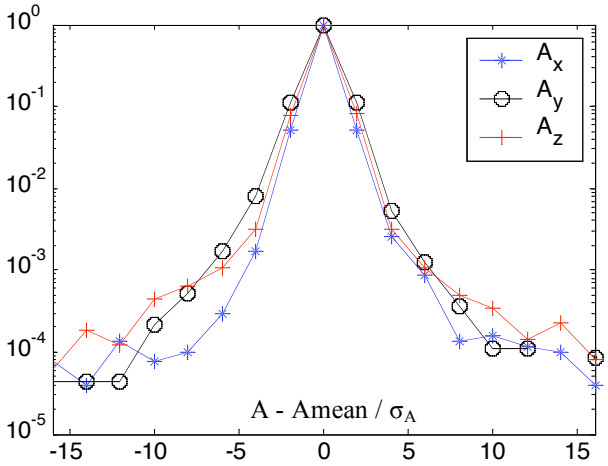

Figure 10: PDF of combined acceleration data.

Figures 11 and Figure 12 show plots of the Lagrangian autocorrelation function in three perpendicular directions for bins R_3 and R_4. Differences in diffusion time scales are evident. The vertical diffusion is greater than that in the horizontal directions. Though we don't have other droplet simulations or experiments to compare with, it agrees with the trends of the Lagrangian simulations performed by Reeks (1997) and the DNS by Squires and Eaton (1991), both of which performed for solid particles. They explain this trend by the continuity effect of "crossing trajectories" (a particle falling from one eddy to another), which decreases the diffusion in the direction perpendicular to gravity to a greater extent, compared to vertical direction. Friedman et al. (2001) show that crossing trajectories is possible for droplets even though their density is lower than that of water.

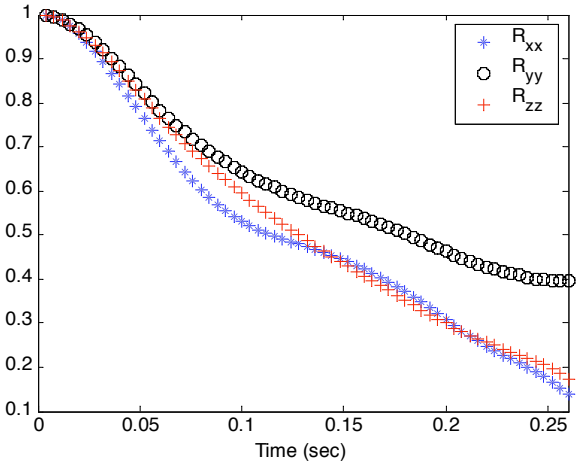

Figure 11: Autocorrelation function for droplets within R_3 (0.45-0.6mm radii) bin in three perpendicular directions (225 rpm).

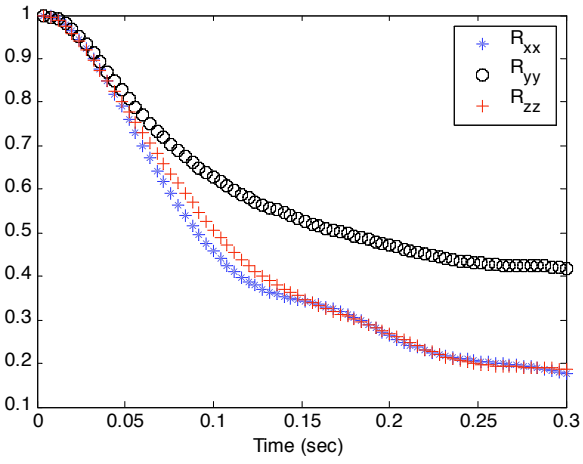

Figure 12: Autocorrelation function for droplets within R_4 (0.6-0.75mm radii) bin in three perpendicular directions (225 rpm).

We average the autocorrelation function in the two horizontal directions (x and z) for droplet bin R_3 (0.45-0.6mm) and use integrate them to get the mean square displacement or dispersion. We also calculate the dispersion for droplet bin R_4 (0.6-0.75 mm) but do not show it, as it closely resembles results of bin R_3. The initial parabolic behavior and the later linear behavior predicted by Taylor's theory are clearly observed for the droplet dispersion in figure 13. Figure 13 also compares droplet dispersion with that of solid particles in air obtained by Snyder and Lumley (1971). Their turbulence rms is three times our value and their particle size is less than the size of their Kolmogorov scale. But it is interesting to note that the dispersion of droplets for times less than 0.25 sec matches with the heavy copper particle. But the slope of these two curves is different and they will deviate for longer times. The dispersion for the vertical direction is not shown as the autocorrelation function is far from reaching zero (data analysis is still in progress), but looking at the autocorrelation we can say that it is going to be significantly higher than that in the horizontal direction.

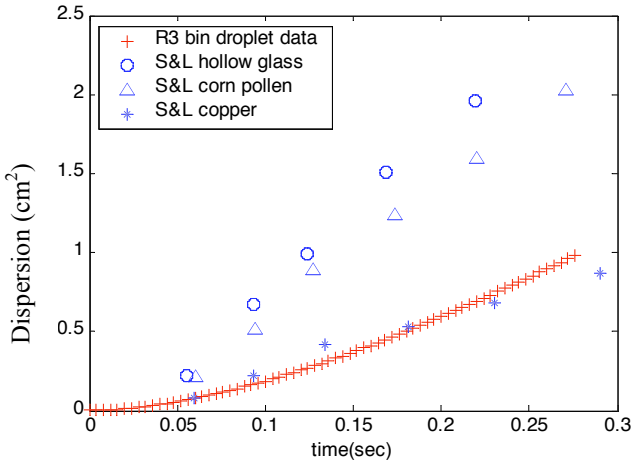

Figure 13: Dispersion in horizontal direction for droplets within R_3 (0.45-0.6mm) bin compared with data from Snyder and Lumley (1971)

Recently, after the DOE contract has expired, we have performed extensive additional experiments for three different rotor speeds (225, 337 and 506 rpm), i.e. different turbulent scales, and for different droplet sizes (0.65, 0.85 and 1.05mm diameter) on the diffusion rate. Note that here we use the diameter of the droplet as size rather than radius, which was used earlier in this report. For this data set, we have enough statistics to determine the droplet rms values of velocity fluctuations, and compare them to those of the surrounding turbulence. Results are summarized in figure 14.

We find that the droplet rms velocity decreases as their size increase. Possible reasons include an increase in drag and increase in particle response time. For the horizontal direction, the droplet rms velocity exceeds that of the fluid rms for all the present range of droplet sizes. Conversely, for the vertical direction, the droplet rms velocity exceeds that of the fluid only for the 0.65mm diameter droplets. For 0.85 and 1.05 mm droplets, the rms value decreases to levels that are lower than the fluid rms.

The diffusion timescale (Figure 15) is obtained by integrating the ensemble averaged droplet velocity covariance normalized by droplet velocity fluctuations

$$T = \int_{\tau=0}^{\infty} \langle U(t)U(t+\tau)\rangle d\tau \,/\, \langle U^2 \rangle$$

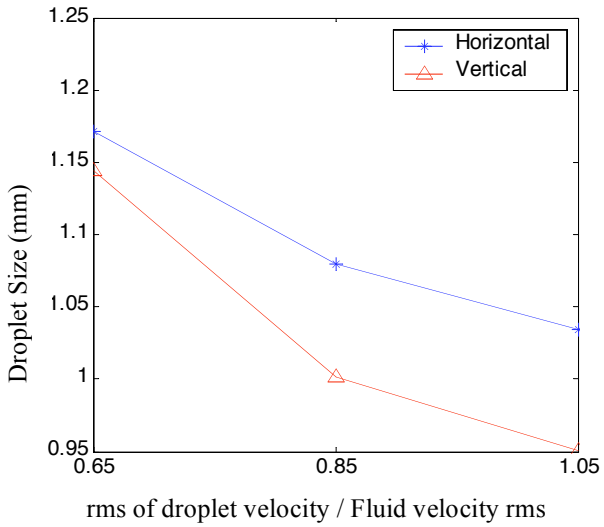

Figure 14: Variation of RMS value of diesel fuel droplet velocity with droplet diameter

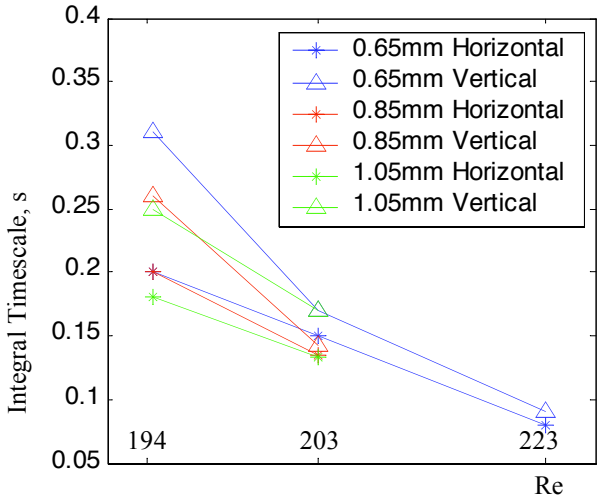

Figure 15: Variation of Droplet Integral timescale with the Taylor Micro-scale Reynolds number of the turbulence (Re), droplet diameter and direction.

As the size of the droplet increases the droplet inertia increases while at the same time the buoyancy force also increases. These competing forces give rise to the observed complicated behavior. For example, in the vertical direction and Re = 203 ($Re=u'\lambda/\nu$) the timescale increases as the size increase from 0.85 to 1.05 mm, conflicting the small but observable trend of timescale decreasing for increasing droplet size. This odd (Re = 203) behavior might be due to high stokes number effects, as this data set has the largest stokes number. The diffusion timescale decreases as the Reynolds number increases primarily due to decrease in turbulence timescales. As observed before, the vertical diffusion timescale is higher than the horizontal diffusion timescale.

Figure 16 shows the variation of diffusion coefficient normalized by fluid rms and fluid integral length scale with droplet size. We can see that diffusion coefficient is almost converged, i.e. the curves almost reach a plateau with increasing time. The diffusion coefficient decreases as the size of the droplet

increases. However this trend is not observed for the largest stokes number case (not shown here) due to the odd timescale behavior mentioned before

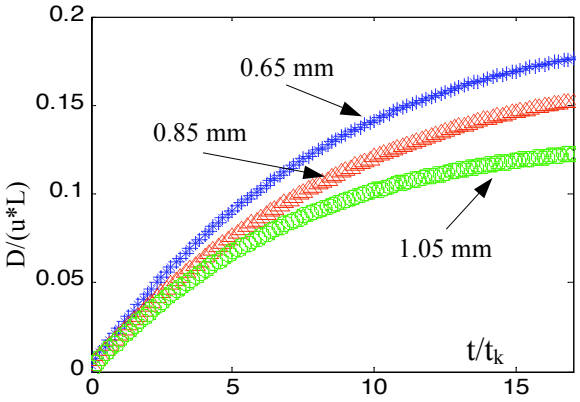

Figure 16: Variation of horizontal Diffusion coefficient, normalized by u'L, with droplet size. t_k is the kolmogorov time scale.

3. ROTATING COUETTE FACILITY FOR MEASURING HYDRODYNAMIC FORCE COEFFICIENTS OF DROPLETS

Construction of the Couette facility for measuring the trajectories of droplets relatively to the surrounding flow has been completed. A sketch and photograph of the facility are presented in figure 17. It consists of two independently rotating, two concentric cylinders that have a maximum speed of 3500 rpm. The facility has been tested for measuring the trajectories of both solid particles in air and droplets/bubbles in water. The flow within the facility has been characterized using PIV. The optical setup for recording four-exposure PIV images by combining two PIV systems, which is needed for acceleration measurements, has also been completed, and is illustrated in figure 18. This system has been tested and sample data has been recorded. Data analysis is currently in progress. Unfortunately, we the project expired before completing this phase.

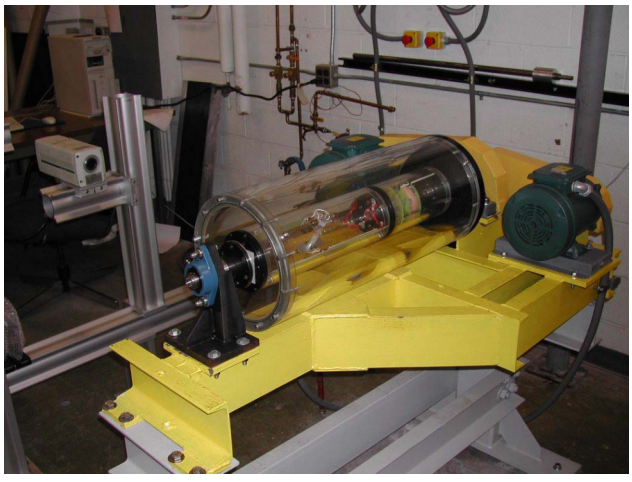

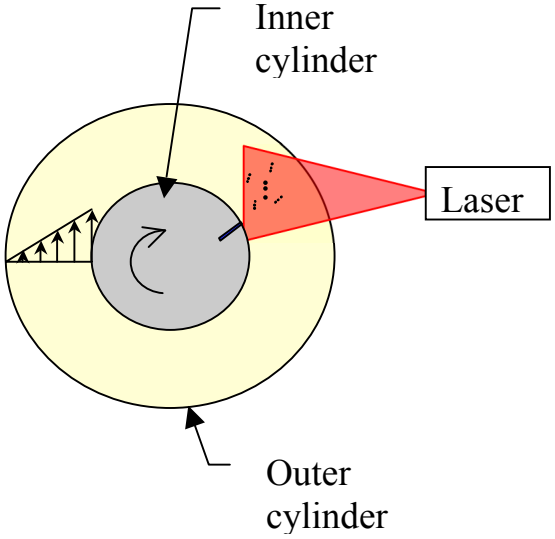

Figure 17: The Couette flow Facility. Right: A sketch of the two concentric cylinders. Left: A photograph of the system.

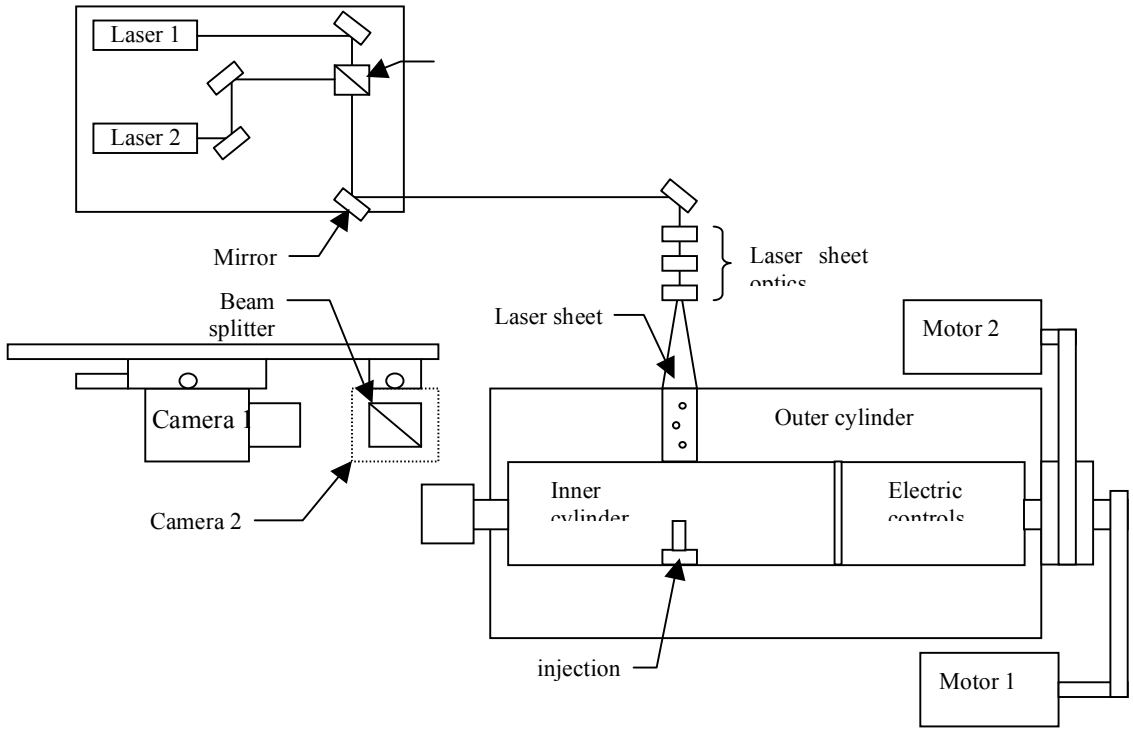

Figure 18: The optical setup for recording four-exposure PIV images on different frames in the Couette facility.

4. NUMERICAL SIMULATIONS

We initially took advantage of existing experimental knowledge base which provided well-established correlations of the forces experienced by bubbles in rotational flow. Based on these correlations, the computational model was used to analyze the rise and scale-dependent dispersion of small air bubbles in isotropic turbulence. As mentioned in Section 1, the flow field is simulated using a pseudo-spectral DNS code, while the particle dynamics are analyzed by integration of a Lagrangian equation of motion with buoyancy, virtual mass, pressure, drag and lift forces. Probability density functions (pdfs) of bubble velocities, lift and drag forces, and of field velocities and vorticities along bubble trajectories were generated, and used to determine bubble dynamics.

Consistent with available experimental data, bubble rise velocities were observed to be increasingly suppressed with increasing turbulence intensity. The analysis also revealed that the vertical bubble velocities are characterized by asymmetric pdfs, that are positive or negative-skewed dependent upon the non-dimensional turbulence intensity and the Taylor length scale. The role of the lift force in moving the bubbles to the down-flow side of turbulent eddies, and consequently retarding their rise, is consistently observed in the computations. Due to buoyancy effects, the pdfs of lift force in the vertical direction are shown to be significantly asymmetric with long negative tails for bubbles larger than 160 μm radius in low turbulence fields.

Lagrangian bubble trajectories are also employed to determine dispersion characteristics, following the theoretical development of Cushman and Moroni (2001). This development was supplemented with a small-wavenumber analysis which enables us to connect, when appropriate, the generalized dispersion predictions with classical dispersion results. Application of the generalized dispersion model to the computed bubble trajectories showed that for small (40μm) bubbles, the dispersion process is initially anomalous, but transitions to Fickian over a time span that scales with the integral time scale of turbulence. This trend persists for the entire range of turbulence levels considered in the analysis. For larger (400μm) bubbles, a qualitatively similar behavior was observed for high turbulence levels. In particular, transition to Fickian dispersion occurs over similar time scales as the small bubbles. At low turbulence levels, however, long-lived oscillations are observed in the generalized dispersion coefficients, which consistent with the "crossing trajectory effect" observed by Snyder and Lumley (1971) and others. Thus, in these situations, transition to Fickian dispersion is not observed within the time span of the analysis.

Computations were finally performed to explain the surprising behavior observed by Friedman and Katz (2002), where rise velocity of droplets smaller than 800μm diameter was enhanced by turbulence whereas the rise of droplets larger than 800μm diameter was retarded. Simulations showed that preferential sweeping due to the lift force to up or down flow sides of turbulent eddies does not explain the observed behavior. A detailed computational study was then conducted to explore whether uncertainty in force coefficients experienced by droplets under high turbulence intensity could explain the observed behavior. The analysis revealed that the observations of Friedman and Katz could only be reproduced if one postulates a rapid drop in drag and virtual mass coefficients when the droplet size is around ten times the Kolmogrov microscale. Thus, the results underscore the difficulties in modeling the motion of small particles under high turbulence intensities, especially when the particle size is close to the turbulence microscale.

A detailed account of the computational study conducted during this project can be found in Snyder et al. (2006) and Snyder (2007).

REFERENCES

Balaji, G., Malkiel, E., Sheng, J., Katz, J., (2005), "Diesel Droplet diffusion in isotropic turbulence with digital holographic cinematography," Paper No. FEDSM2005-77423**,** Proceedings of FEDSM 2005, ASME Fluids Engineering Division Summer Meeting, June 19-23, Houston, TX.

Barnhart, D. H., Adrian, R. J. and Papen, G. C., 1994, "Phase-conjugate holographic system for high-resolution particle image velocimetry." App. Opt., 30, pp. 7159-7170.

Csanady, G. T., 1963, "Turbulent diffusion of heavy particles in the atmosphere," Journal of the Atmospheric Sciences, 20, pp. 201-208.

Friedman, P. D. and Katz, J., 2002, "Mean rise rate of droplets in isotropic turbulence," Physics of Fluids, 14, pp. 3059-3073.

Gopalan, B., Malkiel, E., Katz, J., (2006), "Diffusion of Slightly Buoyant Droplets in Isotropic Turbulence," Paper No. FEDSM2006-98530**,** Proceedings of the ASME, Fluids Engineering Division Summer Meeting, Joint U.S. - European Fluids Engineering Summer Meeting, July 17-20, Miami, FL.

Malkiel, E., Abras, J. N. and Katz, J., 2004, "Automated scanning and measurements of particle distributions within a holographic reconstructed volume," Measurement Science & Technology, 15, pp. 601-612.

Malkiel, E., Sheng, J., Garber, D. and Katz, J., 2004, " An Investigation of Droplet Diffusion in Isotropic Turbulence with Digital Holographic PIV ", ASME Heat Transfer/Fluids Engineering Summer Conference, FED2004-56237.

Moroni, M. and J.H. Cushman, 2001,"Three-dimensional particle tracking velocimetry studies of the transition from pore dispersion to Fickian dispersion for homogeneous porous media". Water Resources Research, 37(4): pp. 873-884

Pu, Y. and Meng, H., 2000, "An advanced off-axis holographic particle image velocimetry (hpiv) system," Experiments in Fluids, 29, pp. 184-197.

Reeks, M W, 1977, "On the dispersion of small particles suspended in an isotropic turbulent fluid "Journal of fluid mechanics.83, pp. 529-546.

Roth, G. and Katz, J., 2001, "Five Techniques for increasing the speed and accuracy of PIV interrogation". Meas. Sci. Technol., 12: pp 238-245

Sheng, J., Malkiel, E. and Katz, J., 2003, "Single beam two-view holographic particle image velocimetry," Applied Optics, 42, pp. 235-250.

Snyder, W. H. and Lumley, J. L., 1971, "Some measurements of particle velocity autocorrelation functions in a turbulent flow," Journal of Fluid Mechanics, 48, pp. 41.

Snyder, M., Knio, O.M., Katz, J. And Le Maitre, O.P., 2006, "Statistical analysis of small bubble behavior in isotropic turbulence," to appear in Physics of Fluids.

Snyder, M., 2007, "Analysis of the behavior of bubbles and droplets in isotropic turbulence," Ph.D. Thesis, Department of Mechanical Engineering, The Johns Hopkins University.

Squires, K.D and Eaton, J.K, 1991, "Measurements of particle dispersion obtained from direct numerical simulations of isotropic turbulence ". Journal of Fluid Mechanics, Vol. 226, p. 1-35

Tao, B., Katz, J. and Meneveau, C., 2002, "Statistical geometry of subgrid-scale stresses determined from holographic particle image velocimetry measurements," Journal of Fluid Mechanics, 457, pp. 35-78.

Taylor, G. I., 1921, "Diffusion by continuous movements," Proc. London Math. Soc., 2, pp. 196-211

Zhang, J., Tao, B. and Katz, J., 1997, "Turbulent flow measurement in a square duct with hybrid holographic PIV," Experiments in Fluids, 23, pp. 373-381.